

# Growth and Characterization of InP Nanowires with InAsP Insertions

Maria Tchernycheva,<sup>\*,†,||</sup> George E. Cirlin,<sup>†,‡</sup> Gilles Patriarche,<sup>†</sup> Laurent Travers,<sup>†</sup> Valery Zwiller,<sup>§</sup> Umberto Perinetti,<sup>§</sup> and Jean-Christophe Harmand<sup>†</sup>

CNRS-LPN, Route de Nozay, 91460 Marcoussis, France, St. Petersburg Physics and Technology Center for Research and Education RAS, Khlopina 8/3, 195220, St. Petersburg, Russia, and Kavli Institute of Nanoscience, Delft University of Technology, P.O. Box 5046, 2600 GA Delft, The Netherlands

Received January 29, 2007; Revised Manuscript Received April 10, 2007

## ABSTRACT

We report on the fabrication by Au-assisted molecular beam epitaxy of InP nanowires with embedded InAsP insertions. The growth temperature affects the nucleation on the nanowire lateral surface. It is therefore possible to grow the wires in two steps: to fabricate an axial heterostructure (at 420 °C), and then cover it by a shell (at 390 °C). The InAsP alloy composition could be varied between InAs<sub>0.35</sub>P<sub>0.65</sub> and InAs<sub>0.5</sub>P<sub>0.5</sub> by changing the As to P flux ratio. When a shell is present, the InAsP segments show strong room-temperature photoluminescence with a peak wavelength tunable from 1.2 to 1.55 μm by adjusting the As content. If the axial heterostructure has no shell, luminescence intensity is drastically reduced. Low-temperature microphotoluminescence performed on isolated single wires shows narrow peaks with a line width as small as 120 μeV.

Free-standing semiconductor nanowires (NWs) attract an increasing attention due to their emerging applications to nanoscale devices such as photoemitters, photodetectors, transistors, etc.<sup>1</sup> A commonly used technique for NW fabrication relies on the catalytic mechanism generally referred to as vapor–liquid–solid (VLS) growth,<sup>2</sup> whereby liquid particles are formed by alloying of the catalyst with the semiconductor constituents. The one-dimensional growth is promoted by the fast local precipitation of adsorbed species at the liquid–semiconductor interface under the droplets. The VLS technique allows the fabrication of heterostructures in both axial and radial directions and to intentionally dope the NWs.<sup>3,4</sup>

The catalytic growth has successfully been applied to synthesize NWs of almost all III–V semiconductors using metalorganic vapor phase epitaxy, chemical beam epitaxy, or molecular beam epitaxy (MBE) growth techniques. A large effort has been devoted to the fabrication of NWs of In(As)P, which is a key material for high-speed electronics<sup>5,6</sup> and for near-infrared light emission/detection applications.<sup>7,8,9</sup> The band gap of InAsP can be tailored from 3.5 to 0.92 μm by adjusting the alloy composition and, in particular, can

cover the 1.3–1.55 μm wavelength range of technological importance for optical telecommunications.

In this letter, we report on the synthesis of InAsP insertions in InP nanowires by Au-assisted MBE. We show that the growth temperature allows us to control the nucleation on the NW lateral surface and provide a method to embed InAsP insertions into InP shells. When a shell is present, the resulting heterostructures demonstrate strong room-temperature photoluminescence with a peak wavelength tunable from 1.2 to 1.55 μm by adjusting the As content. If the axial heterostructure has no shell, luminescence intensity is drastically reduced. The microphotoluminescence performed at 10 K on isolated single wires shows narrow peaks with a line width as small as 120 μeV.

NWs were grown on InP (111)B substrates in an MBE system equipped with solid sources supplying In atoms and cracker As and P sources to produce dimers. The substrate surface was first deoxidized at 530 °C, then a 100 nm thick InP buffer layer was grown to achieve atomically flat surface. A total amount of Au equivalent to 1 nm layer was deposited under phosphorus flux at 420 °C using an Au effusion cell installed directly into the III–V growth chamber. The substrate temperature was then set to the desired value for the growth. This procedure results in the formation of droplets containing Au alloyed with the substrate constituents. The typical distribution of droplet sizes ranges between 30 and 40 nm. After this stage, the NW growth was initiated by opening the In shutter. For all samples, the nominal

\* Corresponding author. E-mail: maria.tchernycheva@lpn.cnrs.fr. Tel: +33169154051. Fax: +33169154115.

† CNRS-LPN.

‡ St. Petersburg Physics and Technology Center for Research and Education RAS.

§ Delft University of Technology.

|| Institut d'Electronique Fondamentale, Université Paris-Sud, 91405 Orsay, France.

growth rate (i.e., the growth rate on a clean and Au-free InP surface) was fixed at 0.2 nm/s.

For InP/InAsP/InP heterostructure formation, the growth started with 20 min of InP, then the As source was opened for 30 s to form an InAsP segment. The As to P flux ratio was varied from sample to sample to investigate different alloy compositions. The growth was completed with 5 min deposition of InP. We did not perform any growth interruption at the heterointerfaces.

The resulting morphology of NW ensembles was investigated by scanning electron microscopy (SEM). The crystallographic structure was analyzed in a transmission electron microscope (TEM) equipped with an energy dispersive X-ray (EDX) spectrometer for composition measurements. For TEM characterization of the NWs, they were either prepared on their substrate by thinning the sample by mechanical polishing and Ar ion milling or separated from their substrate and picked up by touching the substrate with Cu TEM grid with a lacey carbon film. The photoluminescence (PL) of NW ensemble was investigated using the following setup. The sample was excited at normal incidence with 532 nm line of frequency doubled NdYag laser at low excitation density ( $\sim 0.1 \text{ W cm}^{-2}$ ). The luminescence signal was dispersed with a 0.46 m focal length spectrometer and was detected with a nitrogen-cooled Ge photodetector. For micro-PL measurements, NWs were removed from their substrate, dispersed on a SiO<sub>2</sub>/p-Si substrate with the average density of  $\sim 0.1 \text{ NW per } \mu\text{m}^2$ , and placed in a continuous LHe flow cryostat. The light from a semiconductor-based laser ( $\lambda = 532 \text{ nm}$ ) was focused by microscope objective (NA = 0.75) to a spot size of  $\sim 1 \mu\text{m}$  allowing the excitation of a single NW. The signal was collected with the same objective, dispersed with a 0.75 m spectrometer, and detected with a linear array of InGaAs detectors.

First, we investigated the temperature domain where binary InP NWs can be formed. A series of seven samples was grown at temperatures ranging from 330 °C to 440 °C with a constant growth time equal to 20 min. The NW formation was observed only in a relatively narrow temperature window, between 350 and 420 °C. The growth at 330 °C produced only a rough two-dimensional layer that covered the deposited Au catalyst. At 440 °C, the catalyst droplets were found segregating on the growing surface without giving rise to NW formation. In the intermediate range of temperature, NW growth is induced by diffusion of adatoms from the surface to the catalyst droplets and by their subsequent precipitation at the catalyst–semiconductor interface.<sup>10</sup> This mechanism includes the adatom migration along the facets of the NWs as soon as the latter start to grow. The highest average NW growth rate of  $0.7 \pm 0.25 \text{ nm/s}$  was observed for 420 °C. This is 3.5 times greater than the nominal growth rate. The competing growth rate at the bottom surface, which occurs in parallel with the growth of NWs, is  $\sim 0.15 \text{ nm/s}$ .

For temperatures below 410 °C, NWs develop a pencil-like shape. The diameter in the lower part of the wire is two to three times larger than that of the catalyst particle and the NW end is tapered. This morphology indicates that at

low temperatures, concomitantly with the vertical growth governed by the catalyst, the nucleation on the lateral facets also takes place. This phenomenon occurs when the mean diffusion length of species on the lateral NW facets becomes comparable to the NW height. In this case, most of In adatoms supplied by the surface where the NWs stand cannot reach the catalyst droplets. Instead, the species can nucleate on the NW sidewalls giving rise to a significant lateral growth. As suggested by Chen et al.,<sup>11</sup> this growth on the sidewalls may occur in a layer by layer fashion to minimize the steps at the sidewalls surface. As a result, the top of the wires develops tapering to recover the smaller radius of the catalyst particle. On the other hand, one must consider that because of the design of the MBE machine, the molecular beams are not ideally normal to the substrate surface. The incident angles are typically 75° (i.e., a significant part of flux can directly impinge the NW sidewalls). This provides additional species for the step flow of the lateral growth, as well as for maintaining a nonzero axial growth rate, even when the NW length is above the mean adatom diffusion length. These phenomena can explain why along most of their length, the NW have a constant radius, whatever this length is. To reduce the lateral growth, temperature must be raised to increase the adatom diffusion length. At temperatures higher than 410 °C, InP NWs present a cylindrical shape with the diameter equal to that of the catalyst. This means that by raising the substrate temperature it is possible to switch from the mixed axial/lateral growth to almost pure axial growth.

For heterostructure formation, two temperatures corresponding to the two morphologies of InP NWs discussed above were chosen: 390 and 420 °C. Figure 1 a,b shows the SEM top view and cross-sectional image of typical InP/InAsP/InP NWs grown at 390 °C. The resulting NW height is about  $0.75 \mu\text{m}$ , and the diameter varies from 50 to 80 nm. As seen in Figure 1a, the NW cross-section has a hexagonal shape with six facets normal to the [0-11] substrate directions. The InAsP insertion has little influence on the NW morphology, and the NWs present the typical pencil-like shape observed in binary InP NWs grown at this temperature. When the growth proceeds at 420 °C (Figure 1c), the NWs keep a cylindrical shape with 30–40 nm diameter equal to that of the catalyst droplets, a sign that lateral growth is inhibited.

In a third sample, we have intentionally promoted the lateral growth by decreasing the temperature after the InAsP insertion. Figure 1d presents a SEM image of these InP/InAsP/InP NWs that were grown at 420 °C until the formation of InAsP segments was completed. The last 5 min of InP growth was performed at 390 °C. The resulting NW diameter (40–55 nm) is larger than that of the catalyst, especially for long wires, confirming that lateral growth took place.

The size, shape, crystalline structure, and composition of InAsP segments grown at different temperatures were studied by TEM. Figure 2a shows the TEM image of InP/InAsP/InP NW ensemble grown at 390 °C. The pencil-like morphology is clearly seen. The NW crystalline structure is

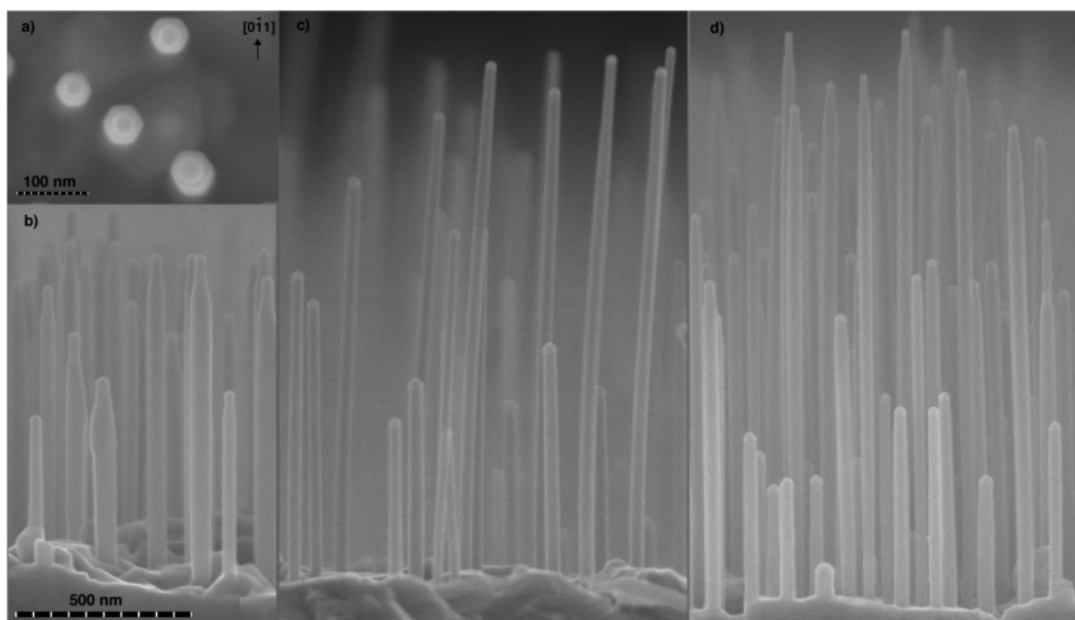


**Figure 1.** (a) Top view SEM image of NWs grown at 390 °C. Cross-sectional SEM images of InP/InAsP/InP NWs grown (b) at 390 °C, (c) at 420 °C, and (d) at 420 °C overgrown with InP at 390 °C. The scale bar is the same for (b–d).

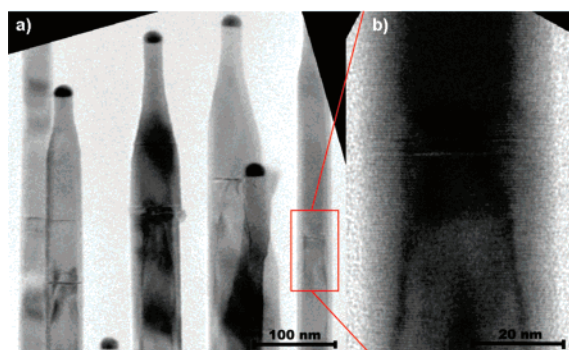


**Figure 2.** (a) TEM image of the InP/InAsP/InP NW ensemble grown at 390 °C. (b) High-resolution TEM image of the InAsP insertion showing 0002 lattice fringes.

wurtzite for both InP and InAsP parts, as commonly observed for VLS grown III–V wires.<sup>12</sup> The viewing direction is oriented parallel to  $\langle 2-1-10 \rangle$  zone axis of the NWs to reveal the stacking faults. The InP parts of the NWs presented less than 1 stacking fault per 500 nm of length. However, in the InAsP insertions stacking faults appeared systematically. Different results were reported by Minot et al.,<sup>9</sup> who observed more stacking faults in InP parts of NWs than in InAsP insertions. Stacking faults and changes in crystal structure from sphalerite to wurtzite are widely observed in III–V NWs. They represent one of the major problems whose origin is still to be clarified. The supersaturation of the III–V constituents in the catalyst phase is probably a key factor. This supersaturation is indeed intimately dependent on the gas-phase conditions, which can strongly vary between growth techniques. In the present heterostructures, switching on and off the P flux is likely to be responsible for transient supersaturation conditions, resulting in stacking faults at proximity of the interfaces. It is important to notice that stacking faults were the only defects present in the structure. No dislocations were observed despite a large misfit (up to

1.6%) between the InAsP insertion and the InP NW lattice parameters. This is consistent with recent calculations showing that the critical thickness of a mismatched layer (i.e., the thickness beyond which interfacial dislocations appear) is larger for a NW than for a two-dimensional layer.<sup>13</sup>

Figure 2b presents a high-magnification image of an InAsP segment. The small difference between the factors of structure of InP and InAsP explains the weak contrast observed in the high-resolution TEM image and makes it difficult to clearly visualize the InAsP segment. Indeed, the contrast is mainly because of the deformation related to the mismatch between the two materials. The strain between InP and InAsP induces a deformation of the atomic planes near interfaces, which locally changes the Bragg condition and thus introduces an additional contrast in the images allowing us to locate the interfaces. To further enhance this strain-induced contrast, the orientation of the NWs was tilted by  $2^\circ$  around the [0001] direction from the  $\langle 2-1-10 \rangle$  zone axis. Figure 3 displays an InAsP insertion observed in these conditions together with a schematic drawing explaining the insertion location. The atomic planes cannot be resolved in that case, but the strain field clearly reveals the interface positions. The segment length and diameter are 27 and 26 nm, respectively. As expected, the InAsP segment is laterally covered with an InP shell formed during the subsequent InP growth. This shell is 7 nm thick. It is noteworthy that a dark region also exists in the NW part below the InAsP insertion; during the catalyzed growth of this segment, a thin layer of InAsP was also deposited on the sidewalls of the pencil-like end of the InP host NW. This dark region (seen in both Figures 2b and 3) reproduces the tapered end of the InP NWs grown at 390 °C.

The EDX spectroscopy was systematically used to determine the composition of InAsP insertions. The measured value was corrected for the presence of InP shell of known

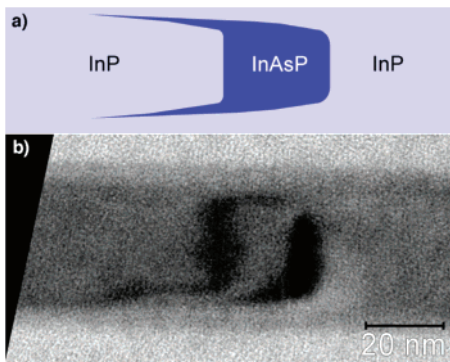


**Figure 3.** (a) Schematic drawing showing the insertion shape. (b) TEM image of InAsP insertion. The orientation of the NW is tilted by  $2^\circ$  around [0001] direction away from the  $\langle 2-1-10 \rangle$  zone axis, which explains the asymmetry of the deformation contrast around the InAsP segment. (The NW growth direction goes from left to right.)

thickness and then averaged over several NWs. The average composition was  $\text{InAs}_{0.35}\text{P}_{0.65}$  for samples grown with As to P flux ratio equal to 1 and  $\text{InAs}_{0.5}\text{P}_{0.5}$  for  $\text{As/P} = 1.5$ . However, important composition fluctuations from wire to wire attaining  $\pm 10\%$  were observed. Size and composition fluctuations from wire to wire can be due to the initial distribution of catalyst particle diameters, as well as their relative position on the surface. The diameter can affect the NW growth rate and its composition; however, experimentally the composition fluctuations were not found to be correlated with the NW diameter. It is possible that shadowing effects, determined by the NW heights and their position relative to each other, lead to significant variations of the effective fluxes impinging the NW sidewalls. This could explain the fluctuations of InAsP insertion composition, as well as the variation of the InP shell thickness.

We have shown that the growth at  $390^\circ\text{C}$  favors the formation of the InP shell around the InAsP segment, but it also produces a thin InAsP foil that extends below the heterointerface. It will be shown below that the InP shell is favorable for the emission properties.<sup>14</sup> However, the presence of the foil is undesirable, as it modifies the shape of the InAsP insertion and makes difficult the precise control of its thickness. The InAsP foil can be almost suppressed by using a higher-growth temperature for InP/InAsP part of the wire. Then the InP shell can be formed by lowering the temperature after the InAsP insertion. Figure 4 shows the TEM image of the InAsP segment synthesized at  $420^\circ\text{C}$  and overgrown by InP at  $390^\circ\text{C}$  during 5 min (SEM image of this sample is shown in Figure 1d). The length and diameter of the inserted InAsP segment are 32 and 27 nm, respectively. The length of the InAsP foil is strongly reduced, and it is clear that the wire end was cylindrical during the growth of the InAsP insertion. The segment presents flat interfaces and is laterally covered with a 10 nm thick InP shell.

The macro-PL measurements were performed on the NW ensembles grown at different temperatures. For samples grown at  $390^\circ\text{C}$  and thus having an InP shell around the InAsP insertions, the luminescence spectra show two peaks

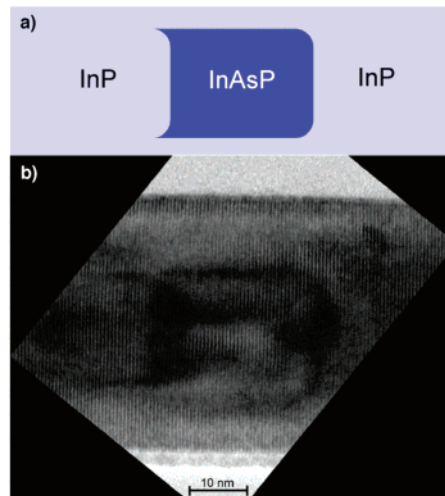


**Figure 4.** (a) Schematic drawing showing the insertion shape. (b) TEM image of InAsP insertion formed at  $420^\circ\text{C}$  and overgrown with InP at  $390^\circ\text{C}$ . (The NW growth axis is directed from left to right.)

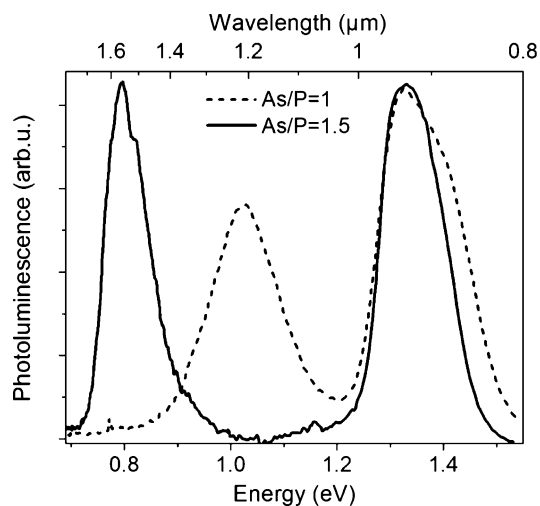


**Figure 5.** Room-temperature PL of InP/InAsP/InP NWs grown at  $390^\circ\text{C}$  with As to P flux ratio equal to 1 (dashed line) and to 1.5 (full line).

(Figure 5). The high-energy peak, situated around 1.35 eV at 300 K with a line width of about 150 meV, has the same position in all the samples. The peak energy corresponds to the bulk InP band gap and should mainly originate from the two-dimensional InP buffer layer with a possible contribution from InP NWs. The large broadening may be explained by a residual concentration of As in InP. The low-energy peak is ascribed to the luminescence of the embedded InAsP segments. To ascertain that this peak does not originate from the emission of the two-dimensional layer, which can still grow between the NWs, we have removed all the NWs from the surface using an ultrasonic bath. After this treatment, the PL spectrum showed only the short wavelength peak; this excludes the possibility of the emission of two-dimensional InAsP layer.

The PL spectra for NW heterostructures grown at  $420^\circ\text{C}$  and overgrown with InP at  $390^\circ\text{C}$  look similar to those of samples grown at  $390^\circ\text{C}$ . However, for samples grown

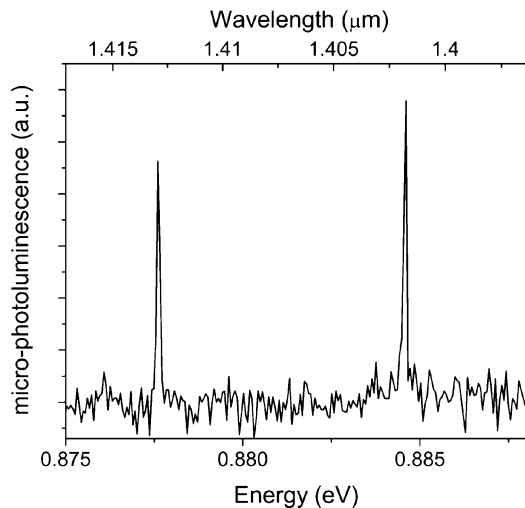


**Figure 6.** Micro-PL spectrum at 10 K of an individual NW containing 2 InAsP insertions of different lengths.

entirely at 420 °C only the high-energy peak at 1.35 eV is present; no emission from the InAsP insertions is observed. This should be related to the suppression of the lateral growth at high temperature. The InP shell acts as an energy barrier that confines the carriers in the InAsP insertion and prevents their diffusion to the NW surfaces. When the InP shell is suppressed, the fast recombination of photogenerated carriers via surface states might hinder the PL emission from InAsP insertions. In addition, the oscillator strength of the exciton is much lower in a shell-free structure because the strain inhomogeneities tend to spatially separate electrons and holes.<sup>15</sup> The InP shell limits the strain relaxation of InAsP insertions, resulting in a better overlap of carrier wave functions.

Figure 5 shows the room-temperature PL spectra of two samples grown at 390 °C with InAsP insertions synthesized at different As to P flux ratio. By changing the As to P flux ratio from 1 to 1.5, the peak emission energy was tuned from 1.025 eV (1.2 μm) to 0.8 eV (1.55 μm). This demonstrates the potential of the InP/InAsP/InP heterostructures for the fabrication of emitters in the telecommunication wavelength range (1.3–1.55 μm). The InAsP peak has an inhomogeneous broadening of 100–150 meV, which should be related to the wire-to-wire composition fluctuations of the InAsP alloy. The room-temperature band gap energies for the observed alloys InAs<sub>0.35</sub>P<sub>0.65</sub> and InAs<sub>0.5</sub>P<sub>0.5</sub> in the zinc-blend phase are 0.98 and 0.828 eV, respectively.<sup>16</sup> Taking into account the uncertainty on the band gap of wurtzite material and the composition fluctuations, the agreement with the observed peak energies is good. It is noteworthy, that the As/P incorporation ratio for MBE-grown NWs is different from the case of CBE. For InAsP NWs grown at 390 °C with tertiarybutylarsine to tertiarybutylphosphine ratio exceeding 50%, the InAs<sub>x</sub>P<sub>1-x</sub> alloy contains more than 80% of As.<sup>17</sup>

Finally, we have performed low-temperature micro-PL measurements on NWs grown at 390 °C containing two InAsP insertions of different lengths (growth time of 30 and 45 s). Figure 6 presents the PL spectrum of an individual

NW measured at 10 K with  $\sim 23$  W/cm<sup>2</sup> excitation density. Two sharp lines attributed to the emission of the InAsP insertions are observed at 1.401 and 1.412 μm with a full width at half-maximum (FWHM) as small as 120 μeV (0.19 nm). The small observed FWHM might be a signature of a quantum dotlike confinement in InAsP insertions. The line width can be expected to be even narrower if we succeed to fabricate smaller InAsP insertions; in the present samples, the sizes of the insertions are larger than the Bohr exciton radius, and quantum confinement should be weak. The effective confining potential is probably reduced by the effect of internal electric field (spontaneous and piezoelectric) that builds up in these heterostructures because the NWs are oriented along the polar <0001> direction.

In conclusion, we have fabricated 27–30 nm high InAsP insertions in InP nanowires by Au-assisted MBE. The wire shape was shown to change from pencil-like for 390 °C growth to cylindrical for 420 °C growth. The alloy composition was adjusted between InAs<sub>0.35</sub>P<sub>0.65</sub> and InAs<sub>0.5</sub>P<sub>0.5</sub> by changing the As to P flux ratio. The presence of InP shells around the InAsP insertions is important to observe efficient PL emission. When a shell is present, the InAsP insertions show room-temperature photoluminescence peaked in the 1.2–1.55 μm wavelength range. The micro-PL from isolated nanowires shows narrow lines with FWHM as small as 120 μeV.

**Acknowledgment.** The financial support of PNANO Filemon35 project, SANDiE European project, and different RFBR grants is acknowledged.

## References

- (1) Li, Y.; Qian, F.; Xiang, J.; Lieber, C. M. *Mater. Today* **2006**, *9*, 19.
- (2) Wagner, R. S.; Ellis, W. C. *Appl. Phys. Lett.* **1964**, *4*, 89.
- (3) Gudiksen, M. S.; Lauhon, L. J.; Wang, J.; Smith, D.; Lieber, C. M. *Nature* **2002**, *415*, 617.
- (4) Lauhon, L. J.; Gudiksen, M. S.; Wang, D.; Lieber, C. M. *Nature (London)* **2002**, *420*, 57.
- (5) Lind, E.; Persson, A. I.; Samuelson, L.; Wernersson, L.-E. *Nano Lett.* **2006**, *6*, 1842.
- (6) Björk, M. T.; Ohlsson, B. J.; Sass, T.; Persson, A. I.; Thelander, C.; Magnusson, M. H.; Deppert, K.; Wallenberg, L. R.; Samuelson, L. *Appl. Phys. Lett.* **2002**, *80*, 1058.
- (7) Duan, X.; Huang, Y.; Cui, Y.; Wang, J.; Lieber, C. M. *Nature* **2001**, *409*, 66.
- (8) Pettersson, H.; Tragårdh, J.; Persson, A. I.; Landin, L.; Hessman, D.; Samuelson, L. *Nano Lett.* **2006**, *6*, 229.
- (9) Minot, E. D.; Kelkensberg, F.; Kouwen, M.; Dam, J. A.; Kouwenhoven, L. P.; Zwiller, V.; Borgstrom, M. T.; Wunnicke, O.; Verheijen, M. A.; Bakkers, E. P. A. M. *Nano Lett.* **2007**, *7*, 367.
- (10) Dubrovskii, V. G.; Cirlin, G. E.; Soshnikov, I. P.; Tonkikh, A. A.; Sibirev, N. V.; Samsonenko, Yu. B.; Ustinov, V. M. *Phys. Rev. B* **2005**, *71*, 205325.
- (11) Chen, C.; Plante, M. C.; Fradin, C.; LaPierre, R. R. *J. Mater. Res.* **2006**, *21*, 2801.
- (12) Tchernycheva, M.; Harmand, J. C.; Patriarche, G.; Travers, L.; Cirlin, G. E. *Nanotechnology* **2006**, *17*, 4025.
- (13) Glas, F. *Phys. Rev. B* **2006**, *74*, 121302.
- (14) Borgström, M. T.; Zwiller, V.; Müller, E.; Imamoglu, A. *Nano Lett.* **2005**, *5*, 1439.
- (15) Niquet, Y. M. *Phys. Rev. B* **2006**, *74*, 155304.
- (16) Vurgaftman, I.; Meyer, J. R.; Ram-Mohan, L. R. *J. Appl. Phys.* **2001**, *89*, 5815.
- (17) Persson, A. I.; Björk, M. T.; Jeppesen, S.; Wagner, J. B.; Wallenberg, L. R.; Samuelson, L. *Nano Lett.* **2006**, *6*, 403.

NL070228L